PHILOSOPHICAL TRANSACTIONS OF THE ROYAL SOCIETY A MATHEMATICAL, PHYSICAL & ENGINEERING SCIENCES

Pyrometallurgical significance of Marangoni flow: mechanism and contributions to processing

The Royal Society

Phil. Trans. R. Soc. Lond. A 1998 **356**, 967-980
doi: 10.1098/rsta.1998.0201

The Royal Society

Pyrometallurgical significance of Marangoni flow: mechanism and contributions to processing

By T. Takasu and J. M. Toguri

Chemical Metallurgy Group, Department of Metallurgy and Materials Science, University of Toronto, 184 College Street, Toronto, Ontario, Canada M5S 3E4

In many pyrometallurgical refining processes, Marangoni convection plays an important role because it enhances the mass transport through the boundary layers. Marangoni flow is created by a surface-tension gradient by means of a compositional gradient or temperature gradient or an electrical potential gradient. A great deal of experimental difficulties exist at high temperatures to observe and to identify Marangoni flow from other competitive phenomena. However, this review discusses the mechanism and contribution of Marangoni flow to the following pyrometallurgical processes; the effect of changing the nitrogen composition on the surface of liquid iron, current efficiency in aluminium electrolysis, inclusion distribution in gas–metal arc welding, and the separation of metal or matte droplets from slag. It is concluded that an understanding of the role of Marangoni flow on the kinetics of these operations is important.

Keywords: metal refining; electrocapillary; aluminium electrolysis; welding

1. Introduction

Pyrometallurgical refining processes are concerned with the extraction of the valuable metals by the removal of impurities at high temperatures. The rate of the refining process invariably involves mass transfer through interfaces. The overall transfer rates are usually limited by mass transport through the boundary layers since the chemical reaction steps at high temperatures are sufficiently rapid.

A possible method to enhance mass transport in the interface region is by inducing Marangoni flow by creating a surface-tension gradient by means of a compositional gradient or temperature gradient or an electrical potential gradient.

A great deal of experimental difficulties exist at high temperatures to observe and to identify Marangoni flow from other competitive phenomena. However, this paper will discuss the mechanism and contribution of Marangoni flow to the following pyrometallurgical processes; the effect of changing the nitrogen composition on the surface of liquid iron, erosion rates of refractory, current efficiency in aluminium electrolysis, inclusion distribution in gas–metal arc welding and the separation of metal or matte droplets from slag.

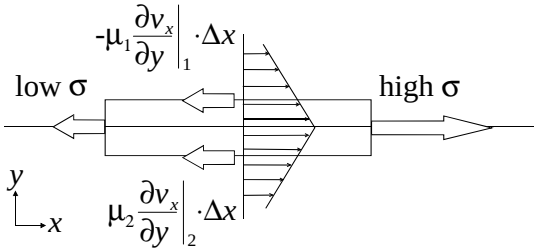

Figure 1. Schematics of the balance of the tangential stress on an interface and the induced flow.

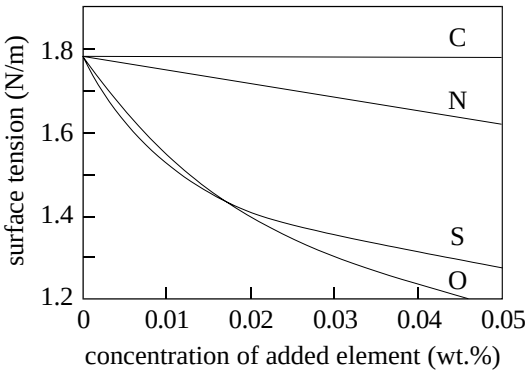

Figure 2. Influence of the addition of minor elements on the surface tension of liquid iron. These results were measured at 1823 K by Kozakevitch & Urbain (1961).

2. Fundamentals

Figure 1 shows the balance of the tangential stress on an interface and the induced flow. The difference in the interfacial tension induces a flow around the interface through the viscocity. The direction of the flow is from a region of low surface tension to a region of high surface tension.

Equation (2.1) is derived by taking a diffential form. The partial differential of the interfacial tension with respect to distance can be replaced by equation (2.2) since the interfacial tension changes with temperature, concentration and electric potential. The gradients of temperature, concentration and potential cause the flow to occur.

$$\frac{\partial \sigma}{\partial x} - \mu_2 \left.\frac{\partial v_x}{\partial y}\right|_2 + \mu_1 \left.\frac{\partial v_x}{\partial y}\right|_1 = 0, \tag{2.1}$$

$$\frac{\partial \sigma}{\partial x} = \frac{\partial \sigma}{\partial T}\frac{\partial T}{\partial x} + \frac{\partial \sigma}{\partial C}\frac{\partial C}{\partial x} + \frac{\partial \sigma}{\partial \phi}\frac{\partial \phi}{\partial x}. \tag{2.2}$$

In pyrometallurgical refining processes, the gradients of temperature and concentration are high because of the high operating temperatures and the existence of mass transport. An electric potential gradient occurs in an electrolysis cell due to the difference in current density. In addition, the application of an electric potential can be an alternative way to control the mass transfer rates when it is not possible to set up the gradients of temperature and/or concentration.

3. Examples in pyrometallurgical processes

(*a*) *Gas–metal refining reactions*

(i) *Background*

Gas–metal reactions are important methods in pyrometallurgy for the removal of impurities such as carbon and nitrogen from steel. The apparent rate of these reactions can be controlled by mass transfer of the impurities in the diffusion layer of the molten metal phase. Induction or gas stirring has been used to enhance the mass transfer.

Previous researchers have reported that Marangoni convection due to concentration gradient of surface active species enhance the apparent reaction rate. The effect of minor elements on the surface tension of liquid iron is shown in figure 2.

Lange & Wilken (1983) observed a vigorous movement on the surface of liquid iron when a low momentum jet of oxygen was blown onto the surface. They explained that this movement was Marangoni convection caused by an oxygen concentration gradient. Mizukami *et al.* (1988) studied the rate of nitrogen removal from molten steel to the gas phase by blowing a reducing gas (H_2) over the liquid surface. They found that under a reducing gas, higher apparent rate constants for nitrogen removal were obtained compared to the use of an inert gas, such as argon. They concluded that hydrogen reacted with the oxygen in the molten steel which resulted in an oxygen concentration gradient. This gave rise to Marangoni convection which enhanced the apparent rate constants. Yamaguchi *et al.* (1992) studied the effect of reductive gas blowing on the rate of the decarburization reaction under vacuum conditions. When the reducing hydrogen gas was blown over the surface of liquid iron during the decarburization process, the apparent decarburization rate constants were greater than the values obtained with argon gas blowing. Again, they attributed the greater decarburization rate constant to Marangoni convection due to the development of an oxygen concentration gradient.

In all the preceding studies, induction or gas stirring was used. Therefore, it is difficult to distinguish between Marangoni enhanced flow and flow as a result of induction or gas stirring under the reported experimental conditions. Nitrogen absorption into a low-oxygen and sulphur-containing liquid iron was chosen as the experimental system by Hirashima *et al.* (Hirashima *et al.* 1995) because mass transfer in the liquid iron phase was known to control the apparent reaction rate under this condition.

(ii) *Experimental*

A detailed description of the arrangement within the reaction tube is shown in figure 3. Liquid iron was contained in a rectangular, parallelepiped, alumina boat ($20 \times 50 \times 40\,\mathrm{mm}^3$). Nitrogen gas was introduced through a lance with an inner diameter of 3 mm onto the iron surface. The gas flow rate was $42 \times 10^{-3}\,\mathrm{m}^3\,\mathrm{s}^{-1}$. Argon and hydrogen gases were used for comparing the fluid motion. This reaction tube was set in a furnace with $MoSi_2$ heating elements. A X-ray system was used to obtain images of the surface movements of liquid iron by using ZrO_2 particles of 1–2 mm diameter as an inert marker. A 5 g sample of iron was taken by suction via a quartz tube which was then quenched in order to determine the nitrogen content in the iron.

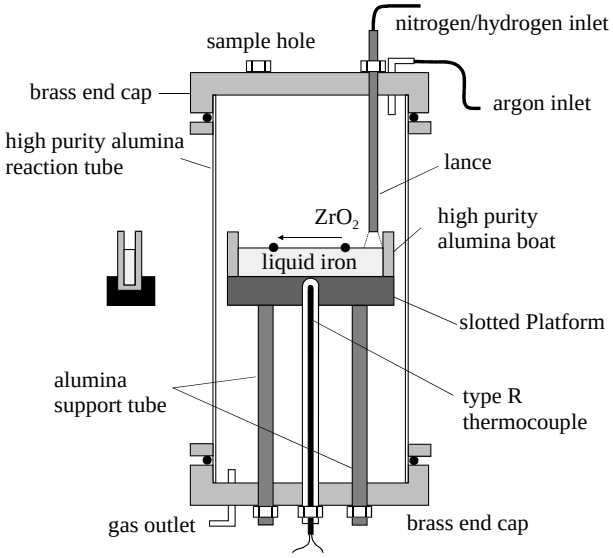

Figure 3. Schematic diagram of the experimental apparatus for nitrogen absorption.

Table 1. *Results of the measured surface motion of liquid iron*

gas	flow rate ($m^3\ s^{-1}$)	lance height (mm)	velocity ($m\ s^{-1}$)	moving direction
N_2	42×10^{-3}	35	0.05 to 0.11	from lance
Ar	42×10^{-3}	35	0	—
H_2	12×10^{-3}	5	0.15 to 0.20	toward lance

(iii) *Results and discussion*

The surface velocity profile in the case of nitrogen gas blowing is shown in figure 4. The direction of flow was from the impingement area to the outer edge. A high concentration of nitrogen at the impingement area leads to a low-surface-tension zone which creates convection from a low-surface-tension area (from the lance) to a high-surface-tension area. The velocity is high in the vicinity of the nitrogen impingement area and decreases on going away from the area. The velocity varies from 0.05 to 0.11 $m\ s^{-1}$. A comparison of the flow using different gases is shown in table 1. No movement on the surface was observed for the case of Ar injection. When H_2 is used as the blowing gas, the direction of flow was opposite to that for the case of N_2 injection. A high concentration of hydrogen at the impingement area leads to a low concentration of oxygen because hydrogen reacts with oxygen in the molten iron. This results in a high-surface-tension zone. A convection was created from a region of low surface tension to a high-surface-tension area (towards the lance). From these results, it is obvious that flow is induced by the surface-tension gradient and not by the momentum of the gases.

Figure 5 shows a plot between At/V ($s\ m^{-1}$) and $\ln([\%N]^i - [\%N]_0)/([\%N]^i - [\%N]_t)$. If the apparent reaction is first order, the slope will indicate the apparent mass transfer coefficient. It was confirmed that at the experimental gas flow rate, the mass transfer coefficient was not affected. This suggests that the concentration

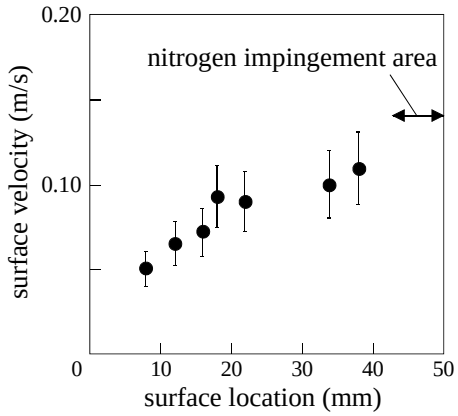

Figure 4. Surface velocity profile in the case of nitrogen gas blowing.

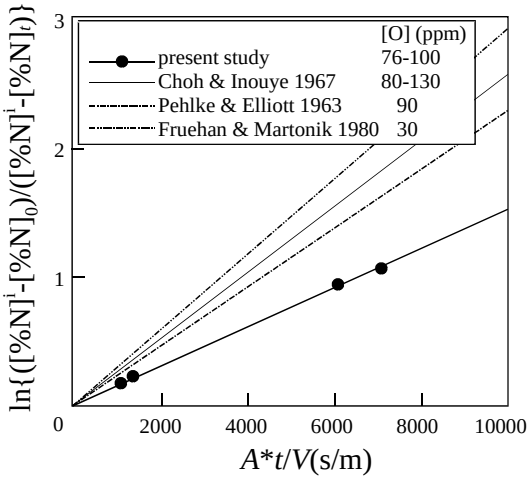

Figure 5. Comparison of the present apparent mass transfer coefficients with reported literature values for nitrogen absorption into low-oxygen and sulphur-containing liquid iron.

at the interface reaches the solubility limit of nitrogen into the iron. It would appear that the electromagnetic force was the main force to induce flow in the case of the experimental data reported in the literature. Under the condition of only Marangoni flow, the mass transfer coefficient is less than that when electromagnetic forces operate. However, because the order of magnitude of the coefficient is similar, Marangoni convection has the potential to enhance the reaction rate.

Calculations were performed assuming such experimental conditions. The results showed good agreement both for velocity and for concentration by taking turbulence into account.

(*b*) *Electrolysis*

(i) *Backgound*

The Hall–Heroult process is widely used to produce primary aluminium from alumina dissolved in molten cryolite by using electrolysis. A dissolution reaction shown in equation (3.1) occurs at the aluminium–bath interface where the electric field is

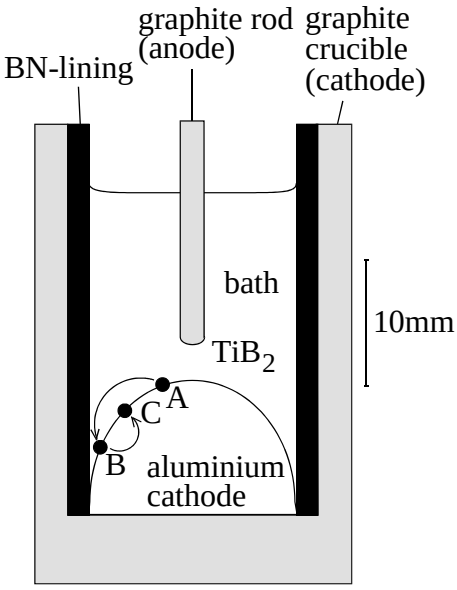

Figure 6. Experimental electrolysis cell and observed movement of particles.

small, and decreases the current efficiency:

$$\mathrm{Al} \rightarrow \mathrm{Al}^{3+} + 3\mathrm{e}^{-}. \tag{3.1}$$

The overall rate of this reaction is generally accepted to be controlled by mass transfer of Al^{3+} into the bath phase. Thus all factors which affect the bath–metal boundary will have an influence on the current efficiency.

(ii) *Experimental*

The experimental electrolysis cell is shown in figure 6. The experiments were carried out in a graphite crucible with an inner diameter of 20 mm. The crucible was lined with boron nitride to prevent passage of current to the side of the crucible. A graphite rod with a diameter of 3 mm was used as the anode. In addition to cryolite, the bath contained 5 mass% CaF_2, 8 mass% AlF_3 and 3 mass% Al_2O_3. Small particles of TiB_2 were used as a marker at the bath–metal interface to serve as movement indicators. X-ray radiography was used to obtain the image of the particles and the interface.

(iii) *Results and discussion*

The effect of the cryolite ratio on the interfacial tension between aluminium and cryolite is shown in figure 7. Most workers have found that the interfacial tension increases with increase in AlF_3 content in the bath.

On applying a positive current (aluminium drop being the cathode) the drop apex increased, indicating an increase in the interfacial tension. The opposite effect was observed when a negative current was applied. This appeared to be an instantaneous effect which indicates that it is associated with charge effects at the interface.

As time proceeded, the effect of the current on the surface tension decreased. Figure 8 shows the change in the surface tension calculated from the observed interface geometry when the current was interrupted. An instantaneous drop in the interfacial tension occurred when the current was interrupted. High values of the interfacial

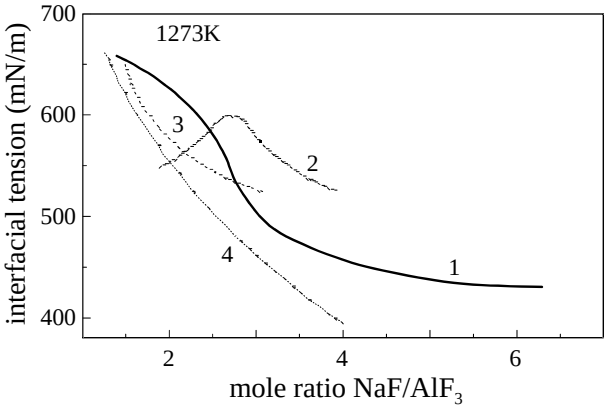

Figure 7. Interfacial tension of aluminium in cryolite melts at 1273 K: 1, Utigrad & Toguri (1985); 2, Gerasimov & Belyaev (1958); 3, Zhemchuzina & Gerasimov (1960); 4, Dewing & Desclaux (1977).

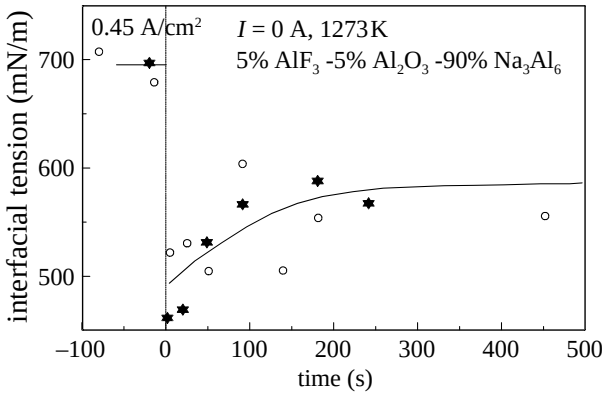

Figure 8. Effect of time after current interruption on the aluminium–cryolite interfacial tension.

tension during the electrolysis is due to the excess negative charge on the aluminium surface. After this sudden drop, the interfacial tension increases with time. This effect is caused by the accumulation of an exess amount of NaF at the interface during electrolysis (Thonstad & Rolseth 1978) and the slow diffusion of NaF away from the interface when electrolysis is stopped.

Figure 6 shows the movement of a particle placed at the bath–metal interface. Before current was applied, the particle rested in position A. Within seconds after a current of 3.1 A was applied (graphite rod anode), the particle began to move towards the wall of the crucible. It travelled the distance from A to B in approximately 1 min. The average speed was 12 μm s^{-1}. The arrest of the particle in position B resulted because it touched the wall of the crucible. The electrolysis was interrupted after 5 min and the cell was disconnected for another 5 min before electrolysis was resumed with reverse polarity (aluminium positive). Movement of the particle was detected after 12 s. It started to move towards position C. This position was reached in 28 s after the current was applied, which leads to an average speed of 13 μm s^{-1}.

The movement was from a region of high to low current density under conditions of 'normal' electrolysis. The boundary layer in the high-current-density region becomes more enriched with NaF than in the region with low current density due to the high

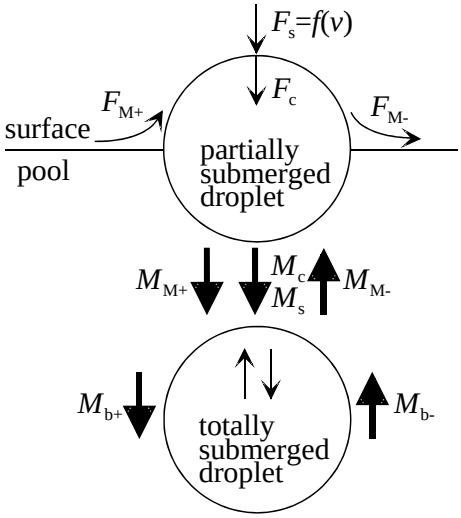

Figure 9. Forces and motions induced when a droplet falls onto a liquid pool.

transference number of sodium ions in cryolite melts. This results in an interfacial tension gradient which drives the interface from the centre to the wall and causes the TiB_2 particle to move down the curved interface. On the other hand, when the 'reverse' current was imposed, the high-current-density region close to the graphite electrode is more depleted in sodium ions and more enriched with aluminium ions than in the low-current-density region closer to the wall of the crucible. Then the particles moved from the wall towards the centre.

The velocity of the particles was rather low mainly due to the small current-density gradient in this system. Calculation for the pratical electrolysis conditions showed an interfacial velocity of 47 mm s^{-1} and a current loss of about 2% due to Marangoni flow.

(*c*) *Inclusion distribution in welding*

(i) *Backgound*

The importance of Marangoni flow has been widely investigated in gas–tungsten arc welding (Heiple & Roper 1982; Walsh & Savage 1985; Oreper *et al.* 1983; Kou & Wang 1985; Zacharia *et al.* 1989). When a filler metal is used, such as in gas–metal arc welding, the Marangoni interaction of the molten filler metal when it touches the weld pool has not been addressed. When there is a difference in the surface tension between filler metal and weld pool, Marangoni flow is important because the surface tension varies when the droplet hits the pool. A water–alcohol physical model was built to study the relative strengths of the driving forces responsible for fluid motion when a liquid droplet falls onto an isothermal liquid bath. There are four forces that are responsible for driving the fluid flow motion in the pool as shown in figure 9: (1) 'stirring' force, F_s, due to the momentum of the free falling droplet onto the pool; (2) 'curvature' force, F_c, due to the component of surface tension normal to the surface; (3) buoyancy force (F_{b+} or F_{b-}) due to the density difference between the droplet and pool; and (4) Marangoni force (F_{M+} or F_{M-}) due to the surface tension difference between the droplet and pool.

Table 2. *Composition of droplets and bulk liquid and their physical properties*

case	droplet	pool	$\sigma_d - \sigma_p$ (mN m^{-1})	$\rho_d - \rho_p$ (kg m^{-3})
1	water	water	0	0
2	3% alcohol	8% alcohol	9.9	8.1
3	water	8% alcohol	22.3	13.7
4	8% alcohol	3% alcohol	−9.9	−8.1
5	34% alcohol	water	−41.0	−53.9
6	water	7.6% NaCl	−2.5	−53.8

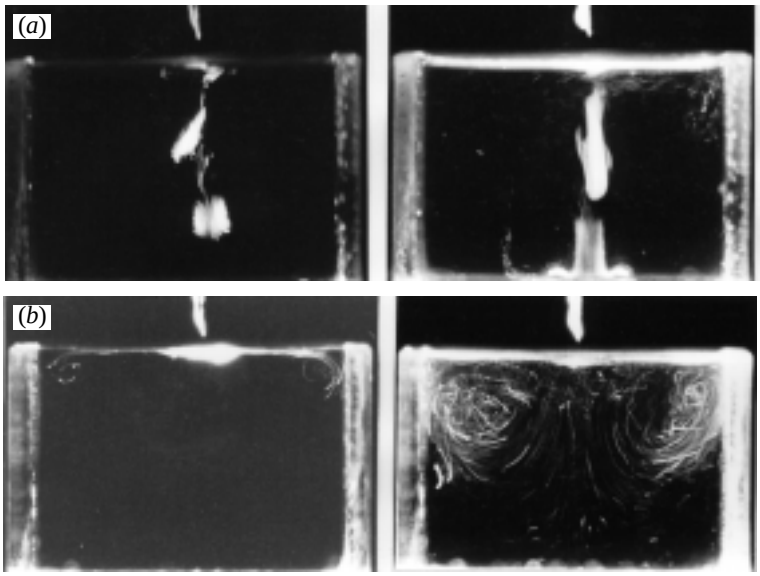

Figure 10. Behaviour of falling drop on a liquid pool.

(ii) *Experimental*

Physical model experiments using water and ethyl alcohol solution were conducted. Flow in the pool was observed by a particle tracking technique using a dark-field illumination method. An acrylic cell, 40 mm long, 20 mm wide and 30 mm high, served as the pool container. Droplets were created by means of a syringe-needle arrangement located 3 mm from the surface. The particles employed for flow tracking were hollow glass spheres (mean size 100 μm diameter).

Table 2 shows the experimental conditions employed and the cases studied.

(iii) *Results and discussion*

In case 1, at $\frac{1}{8}$ s after impact, the drop penetrated up to one-third the depth of the pool. There is no definitive flow being developed in the pool after 1 s. Hence the effects of the stirring force and curvature force on flow development are weak in this experiment.

Figure 10 shows the behaviour of a falling drop on a pool for cases 2 and 3. The droplet penetrates deep into the bath and hits the bottom of the cell within 1 s. The

flow in case 3 is much more intense than in case 2. In order to determine the relative strength of the buoyancy force, the same volume of fluid was introduced slowly into the acrylic cell below the surface of the pool. It was observed that the downward flow velocities due to the buoyancy force were about 30 times smaller than those observed in case 3. Thus, it was ascertained that the deeper penetrating flow in cases 2 and 3 were due primarily to Marangoni forces.

In cases 4 and 5, radially outward surface flows were generated. Definitive toroidal flow was also observed in the bulk fluid as shown in figure 10.

In case 6, the droplet showed about same penetration depth as case 1, but the initial spreading on the surface is not evident. No definitive flow is noticeble at 1 s. Hence the flow observed in cases 4 and 5 is mainly created by the Marangoni effect.

If the surface tension of the droplet is higher than that of the pool, the droplet will penetrate into the pool and the inclusions will segregate at the bottom. On the other hand, if the surface tension of the droplet is lower than that of the pool, the droplet will spread out on the surface and inclusions will segregate near the surface of the weldment.

(*d*) *Separation of metal or matte from slag*

(i) *Backgound*

During the smelting of metal-sulphide concentrates, a two-phase liquid system consisiting of a matte phase and a slag phase is produced. The degree of separation between the two phases is one of the main factors which determines the metal losses of the process. The pay metals (Ni, Cu and Co) are generally lost to the slag phase in two forms: either as dissolved metals or as physically entrapped metal or metal-sulphide droplets. In the majority of cases, the physically entrapped inclusions are the dominant form of pay metal losses.

Two methods of slag cleaning have been employed for reducing pay metal losses to the slag. The first method involves the slow cooling of the slag followed by grinding and concentration of the copper-containing components by flotation. In the second method, the matte and slag are kept molten under reducing conditions in a furnace to allow the heavier sulphide inclusions to settle gravimetrically through the reduced slag into the matte phase. However, there is a limitation to the droplet size when separation is governed by Stokes law: a 0.5 mm diameter matte droplet settles at a rate of about 2 mm s^{-1}, but a 0.1 mm droplet will settle at about 0.07 mm s^{-1}. It is believed that the application of an electric field might assist in the separation process and thus enhance metal recovery.

The electrocapillary phenomenon which moves the droplet is caused by a difference in the interfacial tension due to the electric potential. Figure 11 shows the typical fundamental relationship between the capillary motion and the electrocapillary diagram. If the polarization is ideal (no decomposition) and the solution is of fixed condition, the Lipmann equation gives the relationship between the surface excess charge density and the interfacial tension gradient with respect to the electric potential:

$$\left(\frac{\partial\sigma}{\partial\phi}\right)_{\mu} = -q_{\mathrm{m}}. \tag{3.2}$$

At a potential of zero, $\partial\sigma/\partial\phi$ has a negative value because the metal surface is usually positively charged when no field is applied. A high value of the absolute potential decreases the interfacial tension since the charges repel each other and then reduce

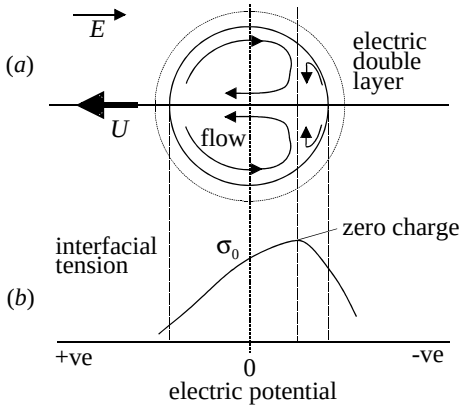

Figure 11. Relationship between (*a*) electrocapillary motion and (*b*) electrocapillary diagram.

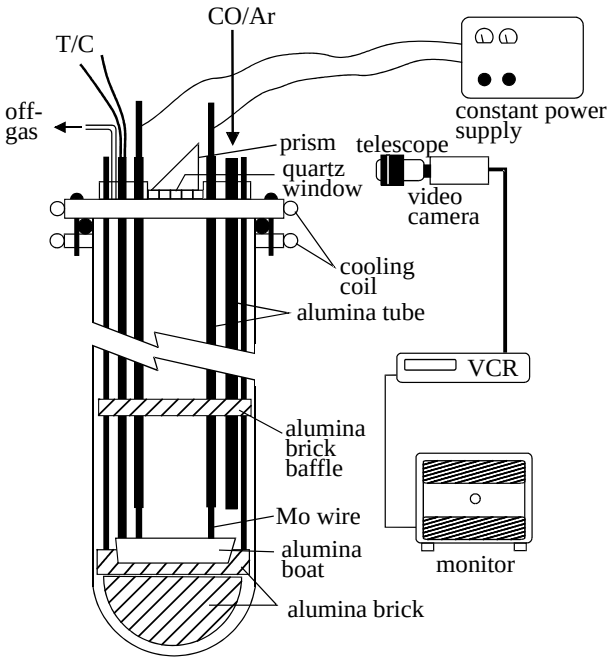

Figure 12. Experimental set-up for droplet migration measurements.

the surface tension. When an electric field is imposed on the droplet, the interfacial tension has a maximum value at the location where the potential corresponds to the maximum in the electrocapillary diagram. Then, two circulating flows are expected. This surface motion of the droplet will also drag adjacent layers of electrolyte. As a result, the entire droplet moves. The direction of the movement depends on the dominant flow which is created by the steeper slope in the electocapillary diagram.

(ii) *Experimental*

Figure 12 is a schematic representation of the experimental set-up. An alumina boat (60 mm by 15 mm) was used as a container for the working slag. A pre-mixed gas mixture of 50% Ar–CO was introduced into the alumina reaction tube. Mo wire electrodes are located at both ends of the boat. A single particle of previously weighed

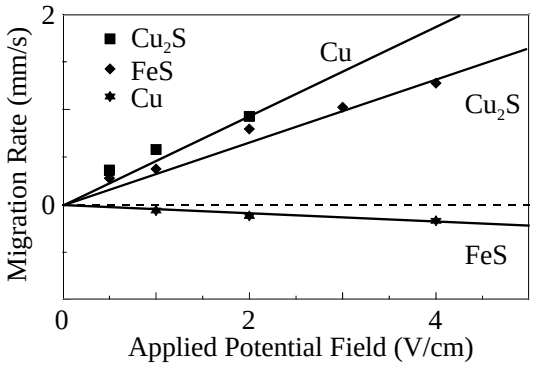

Figure 13. Effect of applied electric field on the migration rates of Cu, Cu_2S (80%Cu) and FeS droplets on the surface of synthetic fayalite slag (70%FeO) at 1523 K.

sulphide was introduced onto the slag surface via a quartz tube. When the particle had melted, which was almost instantaneously, it was kept on the slag surface by surface-tension forces. The droplet migration was observed from above.

(iii) *Results and discussion*

Levich (1962) has derived an equation for the migration rate as shown in equation (3.3):

$$U = \frac{\epsilon E a}{(2\mu + 3\mu')(1 + (a/2\chi\omega)) + (\epsilon^2/\chi)}, \tag{3.3}$$

$$\omega = \frac{RT}{zFi_{\lim}}, \tag{3.4}$$

where ϵ (C m^{-2}) is the surface excess charge density, E (V m^{-1}) is the electric field, a (m) is the droplet radius, μ (Pa s) is the viscosity of the electrolyte, μ' (Pa s) is the viscosity of the droplet, χ (S m^{-1}) is the electrical conductivity of the electrolyte, ω (Ω m^{-2}) is the interfacial resistance, R (j K^{-1} mol^{-1}) is the gas constant, T (K) is temperature, z is valency, F (C mol^{-1}) is Faraday's constant and $i_{\lim}$ (A m^{-2}) is the limiting current density. The term relating to ω in equation (3.3) means that the redox reaction will occur at the interface and the droplet is no longer ideally polarized if the potential exceeds the decomposition potential of the chemical species in the droplet.

Figure 13 shows the migration rates of Cu_2S, FeS and Cu droplets on synthetic fayalite slag. The positive velocity denotes migration to the anode. The migration rate increased with increase in the applied electric field. The direction of migration depends on the material of the droplet. The migration rates of solid Ni, Fe, C and Al_2O_3 were also investigated and these particles remain almost motionless. The intensity of the electrocapillary motion is thought to be higher than that of electrophoresis.

Figure 14 shows the effect of droplet size on the migration rates of Cu_2S droplets on the surface of synthetic fayalite slag. Increase in the droplet size increases the migration rate. This is because the Marangoni force is proportional to the surface area while the viscosity force is proportional to the radius. However, the effect shows the tendency to saturate in the case of larger radius. This effect is thought to be caused by an increase in the decomposition, as expressed in equation (3.3).

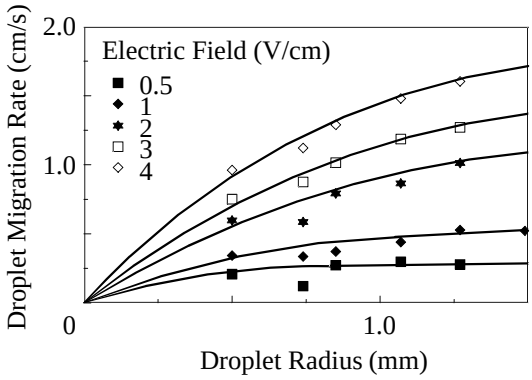

Figure 14. Effect of droplet size on the migration rates of Cu_2S droplet on the surface of synthetic fayalite slag (70%FeO) at 1523 K.

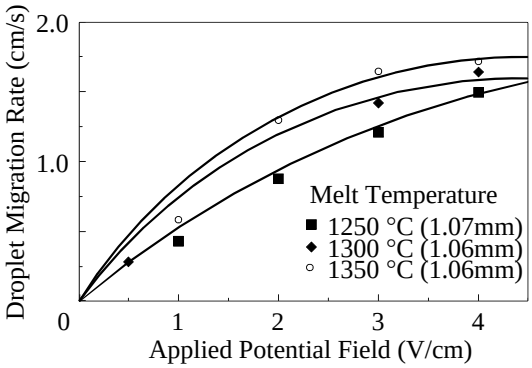

Figure 15. Effect of applied electric field on the migration rates of Cu_2S droplets on the surface of synthetic fayalite slag (70%FeO) at various melt temperatures.

Figure 15 shows the effect of temperature on the migration rate. The migration rate increases with increase in temperature. This is in accordance with equation (3.3) where the higher temperatures result in lower slag viscosities and higher electrical conductivities.

4. Summary

The mechanism and contribution of Marangoni flow to the following pyrometallurgical processes are discussed: the effect of changing the nitrogen composition on the surface of liquid iron, current efficiency in aluminium electrolysis, inclusion distribution in gas–metal arc welding, and the separation of metal or matte droplets from slag. It was shown that the Marangoni flow affects the mass transport of dissolved materials, inclusions or droplets. An understanding of the role of Marangoni flow on the kinetics of these operations is important. Further effort should be directed to investigate whether Marangoni convection occurs in current industrial processes in order to advantageously maximize the use of this phenomenon and also to develop new processes based on the application of Marangoni flow.

References

Choh, T. & Inouye, M. 1967 *Tetsu-to-Hagane* **53**, 1393-1406.

Choo, R. T. C., Warczok, A. & Toguri, J. M. 1991 Experimental studies of the electrodynamic behaviour of metal and metal sulphide droplets in slag. In *Pyrometallurgy of Copper, Copper 91-Cobre 91* (ed. C. Diaz, C. Landolt, A. Luraschi & C. J. Newman), vol. 4, pp. 409–424. CIM, Pergamon Press.

Choo, R. T. C. & Toguri, J. M. 1992 *Canadian Metall. Q.* **31**, 113–126.

Choo, R. T. C., Mukai, K. & Toguri, J. M. 1992 *Welding Res. Suppl.* **71**, 139s–146s.

Dewing, E. W. & Desclaux, P. 1977 *Met. Trans.* B **8**, 555–561.

Fruehan, R. J. & Martonik, L. J. 1980 *Tetsu-to-Hagane* B **11**, 615–621.

Gerasimov, A. D. & Belyaev, A. I. 1958 *Izv. Vyssh. Uchebn. Zaved, Tsvet. Met.* **1**, 58.

Heiple, C. R. & Roper, J. R. 1982, *Welding J.* **61**, 97s–102s.

Hirashima, N., Choo, R. T. C., Toguri, J. M. & Mukai, K. 1995 *Metall. Mater. Trans.* B **26**, 971–980.

Itoh, S., Choo, R. T. C. & Toguri, J. M. 1995 *Canadian Metall. Q.* **34**, 319–330.

Kou, S. & Wang, Y. H. 1985 *Welding J.* **65**, 63s–70s.

Kozakevitch, P. & Urbain, G. 1961 *Mem. Sci. Rev. Metall.* **58**, 931–947.

Lange, K. W. & Wilken, M. 1983 *Can. Metall. Q.* **22**, 321–326.

Levich, V. G. 1962 *Physicochemical hydrodynamics*, pp. 472–531. Englewood Cliffs, NJ: Prentice-Hall.

Mizukami, Y., Mukawa, S., Saeki, T., Shima, H., Onoyama, S., Komai, T. & Takaishi, S. 1988 *Tetsu-to-hagane* **74**, 294–301.

Oreper, G. M., Eagar, T. W. & Szekely, J. 1983 *Welding J.* **62**, 307s–312s.

Pehlke, R. D. & Elliott, J. F. 1963 *Trans. AIME* **227**, 844–855.

Thonstad, J. & Rolseth, S. 1978 *Electrochim. Acta* **23**, 223–241.

Utigard, T. & Toguri, J. M. 1985 *Met. Trans.* B **16**, 333–338.

Utigard, T. & Toguri, J. M. 1986 *Met. Trans.* B **17**, 547–552.

Utigard, T. & Toguri, J. M. 1990 Marangoni flow in the Hall–Heroult cell. In *Light Metals 1991* (ed. E. L. Rooy), pp. 273–281. The Minerals, Metals and Materials Society.

Utigard, T., Rolseth, S., Thonstad, J. & Toguri, J. M. 1989 Interfacial phenomena in aluminum electrolysis. In *Proc. Int. Symp. on Production and Electrolysis of Light Metals, Halifax* (ed. B. Closset), pp. 189–199. Pergamon Press.

Walsh, D. W. & Savage, W. F. 1985 *Welding J.* **64**, 59s–62s.

Yamaguchi, K., Takeuchi, S. & Sakuraya, T. 1992 *CAMP-ISIJ* **5**, 1274.

Zacharia, T., David, S. A., Vitek, J. M. & Debroy, T. 1989 *Welding J.* **68**, 499s–519s.

Zhemchuzhina, E. A. & Belyaev, A. I. 1960 Interfacial tension at the boundary between liquid Al and molten salts. *Fiz. Kim. Rasplav. Soleii Shlakov, Akad Nauk SSSR, Uralsk Filial, Inst. Elextrochim., Tr. Vses. Soveshch., Sverdlovsk*, pp. 207–214.